

Structure and interstitial deuterium sites of β -phase ZrNi deuteride

H. Wu,^{1,2,*} W. Zhou,^{1,3} T. J. Udovic,¹ J. J. Rush,^{1,2} T. Yildirim,^{1,3} Q. Huang,¹ and R. C. Bowman, Jr.⁴

¹*NIST Center for Neutron Research, National Institute of Standards and Technology, 100 Bureau Dr., MS 8562, Gaithersburg, Maryland 20899-8562, USA*

²*Department of Materials Science and Engineering, University of Maryland, College Park, Maryland 20742-2115, USA*

³*Department of Materials Science and Engineering, University of Pennsylvania, 3231 Walnut St., Philadelphia, Pennsylvania 19104-6272, USA*

⁴*Jet Propulsion Laboratory, California Institute of Technology, Pasadena, California 91109, USA*

(Received 15 November 2006; revised manuscript received 21 December 2006; published 9 February 2007)

β -ZrNiD_{1-x} (for $x \approx 0.1$, near the β - γ phase boundary) was found to possess a triclinic $P\bar{1}$ structure as determined by high-resolution neutron powder diffraction. This is very different from the widely accepted orthorhombic and distorted orthorhombic $Cmcm$ structures previously proposed. In contrast to the single type of D site associated with these latter structures, the true β -ZrNiD_{1-x} structure contains two crystallographically distinct interstitial D sites: “Zr₄Ni₂” octahedral sites and “Zr₄” tetrahedral sites, alternately ordered along the a direction. From first-principles calculations, the total energy of the $P\bar{1}$ structure was found to be ≈ 0.24 eV per unit cell lower than $Cmcm$ -symmetry ZrNiD and could be rationalized in terms of different D local-bonding configurations and metal-deuterium interactions. Resultant phonon calculations based on this structure were also consistent with the measured neutron vibrational spectrum.

DOI: 10.1103/PhysRevB.75.064105

PACS number(s): 61.12.-q, 63.20.-e, 71.15.Mb, 71.20.-b

I. INTRODUCTION

The hydrides of the intermetallic ZrNi alloy have been widely investigated concerning their crystal and electronic structures,¹⁻⁶ interstitial-site occupancies,^{3,7-12} thermodynamic properties,¹³⁻¹⁶ and many important technological applications.¹⁷⁻²⁰ Numerous studies have suggested that the α -phase ZrNi metal lattice retains essentially the same structure ($Cmcm$ symmetry) during hydrogen absorption, forming β -phase ZrNiH (i.e., monohydride) and γ -phase ZrNiH₃ (i.e., trihydride).^{1-4,6} The structure and interstitial occupancies of γ -ZrNiH₃ have been exhaustively studied,^{2,6,12} and all the experimental results agree well with the model first proposed by Westlake.⁷ For β -ZrNiH, an early neutron powder diffraction (NPD) study³ and a more recent x-ray diffraction (XRD) study⁶ both favored a structure (α , β , γ within the vicinity of 90°) that can be derived by slightly distorting the $Cmcm$ -symmetric structure. For more than two decades, this quasi- $Cmcm$ structural model has been widely accepted, leading to the conclusion that there is only one type of energetically stable interstitial site (“Zr₄” or better described later as the “Zr₄Ni₂” site) in β -ZrNiH which satisfies the two geometric criteria of minimum hole size and minimum H-H distance.^{3,6,7,9,21} However, a very recent multiprobe study of β -ZrNiD_{1-x} by NMR, XRD, NPD, and neutron vibrational spectroscopy (NVS), which involved some of the present authors,¹² was found to be inconsistent with the previously proposed structural model. This study concluded that there are at least two different interstitial sites occupied, and although the detailed structure could not be determined, both XRD and NPD powder-pattern data could be completely indexed assuming a more highly distorted unit cell with $P1$ symmetry.

In this paper, we report the true crystal structure of β -ZrNiD_{1-x} at $x \approx 0.1$ (i.e., close to the β - γ phase boundary), which was successfully solved and corroborated via a com-

ination of NPD, NVS, and first-principles total energy and phonon calculations.

II. MATERIALS AND METHODS

The sample investigated in the present study had an overall stoichiometry of ZrNiD_{0.88}, and was the same sample identified as JPL-14 in Ref. 12. Sample preparation is described in detail therein. In order to solve the structure, an additional mixed-isotope ZrNi(H_{0.64}D_{0.36})_{0.88} was also synthesized in a similar manner as ZrNiD_{0.88} using α -ZrNi (from the same alloy ingot)¹² hydrided with the appropriate amount and isotopic ratio of H₂/D₂ gas. Due to the positive and negative neutron scattering lengths for H and D, respectively, their contributions to the Bragg peaks nearly cancel out and the resulting powder diffraction is sensitive only to the metal atoms. In this way, we were able to determine the metal positions first and then locate the deuterium atom positions in the actual ZrNiD_{0.88} sample.

All neutron measurements were undertaken at the NIST Center for Neutron Research. The NPD measurements were performed with the BT-1 high-resolution powder diffractometer²² using the Cu(311) monochromator at a wavelength of 1.5403(2) Å. Rietveld structural refinements were done using the GSAS package.²³ The NVS measurements were performed with the BT-4 Filter-Analyzer Neutron Spectrometer²⁴ using the Cu(220) monochromator.

First-principles calculations were performed within the plane-wave implementation of the generalized gradient approximation to density functional theory (DFT) using the PWscf package.²⁵ We used a Vanderbilt-type ultrasoft potential with Perdew-Burke-Ernzerhof exchange correlation. A cutoff energy of 408 eV and a $6 \times 6 \times 6$ k -point mesh were found to be enough for the total energy and force to converge within 0.5 meV/atom and 0.005 eV/Å. Structure optimiza-

tions were performed with respect to lattice parameters and atomic positions. The phonon calculations were conducted with the optimized structure using the supercell method with finite difference.^{26,27}

III. RESULTS AND DISCUSSION

Neither of the structures proposed in previous NPD and XRD studies, $Cmcm$ ($a=3.28$ Å, $b=10.12$ Å, $c=4.05$ Å) (Ref. 3) nor triclinic ($a=3.33$ Å, $b=10.18$ Å, $c=4.03$ Å, $\alpha=89.18^\circ$, $\beta=89.6^\circ$, and $\gamma=89.43^\circ$) (Ref. 6) symmetries were able to fit all the reflections of the current NPD pattern for $ZrNiD_{0.88}$. Rather, as mentioned earlier, the reflections were recently determined¹² to fit a triclinic $P1$ (No. 1) unit cell with lattice parameters: $a=5.2637(1)$ Å, $b=5.3752(2)$ Å, $c=5.2264(1)$ Å, $\alpha=101.521(3)^\circ$, $\beta=100.663(2)^\circ$, and $\gamma=100.590(3)^\circ$ at 300 K, and $a=5.2540(1)$ Å, $b=5.3696(2)$ Å, $c=5.2164(1)$ Å, $\alpha=101.573(3)^\circ$, $\beta=100.633(2)^\circ$, and $\gamma=100.638(3)^\circ$ at 10 K. Using these lattice parameters as a starting point in conjunction with NPD measurements of $ZrNiD_{0.88}$, the true β -phase structure was solved in the following way. The number of metal atoms in our triclinic unit cell (4 Zr and 4 Ni per unit cell) was assumed by comparing its cell volume ($V=138.606$ Å³) to that of $Cmcm$ α -ZrNi ($V_{ZrNi}=134.2$ Å³) (Ref. 3) and the Zr:Ni=1:1 stoichiometry. The NPD pattern for $ZrNi(H_{0.64}D_{0.36})_{0.88}$ was used to initially approximate the positions of the metal atoms, since the coherent scattering intensities from the H/D atoms were largely precluded by the zero sum contributions of the H and D neutron scattering lengths of -3.7406 fm and 6.671 fm, respectively. In turn, the D atom positions were initially approximated by consideration of the possible interstitial-site sizes coupled with the observed intensity differences between the NPD data for $ZrNi(H_{0.64}D_{0.36})_{0.88}$ and $ZrNiD_{0.88}$. The final positions of all atoms were then refined together with the lattice parameters, thermal factors, and D atom occupancies, using the NPD data for $ZrNiD_{0.88}$. The diffraction pattern also revealed a small amount of Zr_9Ni_{11} phase [2.19(1) wt.%, $P4/m$ structure²⁸ with $a=9.907(6)$ Å and $c=6.587(8)$ Å at 300 K, and $a=9.880(7)$ Å and $c=6.585(8)$ Å at 10 K] and α -ZrNi phase [1.05(1) wt.%, $Cmcm$ structure²⁹ with $a=3.30401(6)$ Å, $b=9.8611(2)$ Å and $c=4.08520(5)$ Å at 300 K, and $a=3.303(1)$ Å, $b=9.831(4)$ Å and $c=4.080(2)$ Å at 10 K]. The coexistence of the intermetallic and metal-deuteride phases agrees with previous TEM observations.⁶

The initial refinement results revealed that the crystallographically distinct sites in the $P1$ unit cell were in fact related by an inversion symmetry operation. Therefore, the structural symmetry group could actually be increased from $P1$ to $P\bar{1}$. The final $P\bar{1}$ refinement, including all three phases, yielded excellent agreement factors of $R_{wp}=0.0331$ and $R_p=0.0270$ at 300 K, and $R_{wp}=0.0353$ and $R_p=0.0282$ at 10 K. The experimental, fitted, and difference profiles associated with the 300 K NPD data are shown in Fig. 1. The associated crystallographic and structural parameters are summarized in Tables I and II. The selected bond distances and bond angles

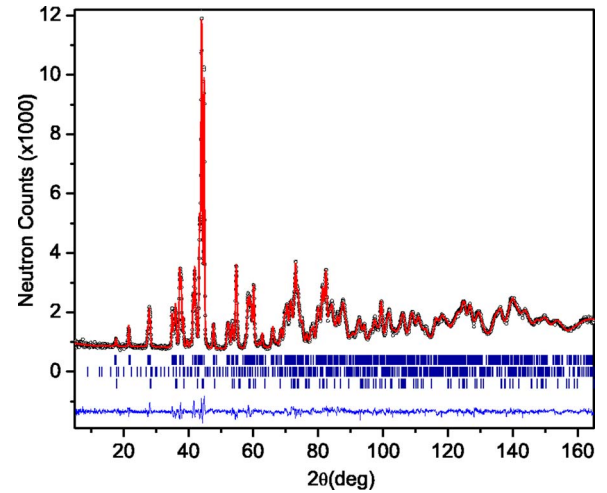


FIG. 1. (Color online) Experimental (dots), calculated (line), and difference NPD profiles for $ZrNiD_{0.88}$ at 300 K. Vertical bars indicate the calculated positions of Bragg peaks for β - $ZrNiD_{1-x}$, Zr_9Ni_{11} , and α -ZrNi (from the top).

are provided in Table III.

An actual β -phase stoichiometry of $ZrNiD_{0.918}$ [i.e., $x=0.082(8)$] is derived from the refined deuterium site occupancies. This is consistent with the fact that $\approx 3.3\%$ of the metal atoms in the $ZrNiD_{0.88}$ sample are found to be part of the trace Zr_9Ni_{11} and α -ZrNi impurity phases. Hence, it should be stressed that the parameters reported in this paper refer to the refined β - $ZrNiD_{0.918}$ stoichiometry rather than the overall $ZrNiD_{0.88}$ stoichiometry. The refined structures at 10 K and 300 K indicate that the lattice parameters, bond lengths, and thermal factors systematically increase with elevated temperature, with no significant structural changes. The crystal structure of this triclinic β - $ZrNiD_{1-x}$ phase is shown in Fig. 2.

In our refined structure, the unit cell contains two different types of deuterium sites. The D1 site (2 per unit cell) is coordinated by 4 Zr and 2 Ni atoms, forming a distorted

TABLE I. Lattice parameters, cell volume, weighted (R_{wp}) and point (R_p) R factors and χ^2 (i.e., goodness of fit) for the refined “ β - $ZrNiD_{0.918}$ ” phase from NPD data at two different temperatures.

Space group ($P\bar{1}$, No. 2)	$ZrNiD_{0.88}$ sample	
	10 K	300 K
T (K)		
a (Å)	5.2540(1)	5.2637(1)
b (Å)	5.3696(2)	5.3752(2)
c (Å)	5.2164(1)	5.2264(1)
α (°)	101.573(3)	101.521(3)
β (°)	100.633(2)	100.663(2)
γ (°)	100.638(3)	100.590(3)
V (Å ³)	137.895(10)	138.606(8)
R_{wp}	0.0353	0.0331
R_p	0.0282	0.0270
χ^2	2.165	1.861

TABLE II. Crystallographic parameters, including site occupancies, fractional coordinates, and thermal factors for the refined " β -ZrNiD_{0.918}" phase within the ZrNiD_{0.88} sample at $T=300$ K and $T=10$ K.

Atom	Site	Occupancy	x	y	z	U_{iso} ($\times 100 \text{ \AA}^2$)
Zr1	2i	1.00	0.2198(6)	0.2929(4)	0.9184(5)	0.40(3)
Zr2	2i	1.00	0.6744(5)	0.2695(4)	0.4635(5)	0.51(4)
Ni1	2i	1.00	0.1212(3)	0.1484(3)	0.3732(3)	0.25(3)
Ni2	2i	1.00	0.2999(4)	0.8550(3)	0.0517(3)	0.13(3)
D1	2i	0.882(6)	0.0290(7)	0.6227(6)	0.7776(9)	1.62(5)
D2	2i	0.954(2)	0.5002(6)	0.4888(5)	0.7423(7)	1.90(5)
Zr1	2i	1.00	0.2186(6)	0.2905(4)	0.9163(4)	0.10(2)
Zr2	2i	1.00	0.6728(5)	0.2691(4)	0.4636(5)	0.14(3)
Ni1	2i	1.00	0.1189(3)	0.1489(3)	0.3722(3)	0.02(2)
Ni2	2i	1.00	0.2991(4)	0.8529(3)	0.0506(3)	0.05(1)
D1	2i	0.880(1)	0.0295(7)	0.6251(5)	0.7815(7)	0.81(9)
D2	2i	0.955(1)	0.5020(6)	0.4913(5)	0.7398(6)	1.27(9)

Zr₄Ni₂ octahedron. This D position is similar to the Zr₄Ni₂ interstitial site previously proposed for β -ZrNiH (Ref. 21) but with much shorter Ni-D1 bond lengths [i.e., 1.810(4) Å and 1.876(4) Å]. The nearest Ni atoms of the D2 site per-

form small concerted displacements towards the two neighboring Zr₄Ni₂ octahedra (D1 sites) so that the Ni-D2 distances are significantly stretched to 2.602(4)–2.779(4) Å, while the Ni-D1 distances in the Zr₄Ni₂ octahedra (D1 site)

TABLE III. Selected bond distances (Å) and bond angles (°) for the refined " β -ZrNiD_{0.918}" phase (300 K).

	Bond length		Bond angle		Bond angle
Zr ₄ Ni ₂ -Site					
D1-Zr1	2.365(5)	Zr1-D1-Ni1	172.72(26)	Zr1-D1-Zr1	81.92(11)
D1-Zr1	2.269(4)	Zr1-D1-Ni2	85.22(20)	Zr1-D1-Zr2	94.30(16)
D1-Zr2	2.247(5)	Zr1-D1-Zr2	87.22(15)	Zr1-D1-Ni1	84.04 (17)
D1-Zr2	2.470(4)	Zr1-D1-Zr2	154.76(16)	Zr1-D1-Ni2	82.45(17)
D1-Ni1	1.810(4)	Zr2-D1-Ni1	87.78(19)	Zr2-D1-Zr1	95.34(16)
D1-Ni2	1.876(4)	Zr2-D1-Ni2	170.99(24)	Zr2-D1-Zr2	105.15(18)
		Ni1-D1-Ni2	100.18(17)	Zr2-D1-Ni1	80.87(20)
				Zr2-D1-Ni2	80.47(15)
Zr ₄ -site					
D2-Zr1	2.110(4)	Zr1-D2-Zr1	100.37(18)		
D2-Zr1	2.064(5)	Zr1-D2-Zr2	111.82(20)		
D2-Zr2	2.135(4)	Zr1-D2-Zr2	119.81(15)		
D2-Zr2	2.079(5)	Zr2-D2-Zr1	109.01(17)		
Nearest Ni		Zr2-D2-Zr1	110.56(16)		
D2-Ni1	2.622(4)	Zr2-D2-Zr2	105.21(19)		
D2-Ni1	2.761(4)				
D2-Ni2	2.602(4)				
D2-Ni2	2.779(4)				
D1-D1	2.872(8)				
D1-D1	2.929(9)				
D1-D2	2.706(7)				
D1-D2	2.734(6)				
D2-D2	2.559(7)				
D2-D2	2.672(7)				

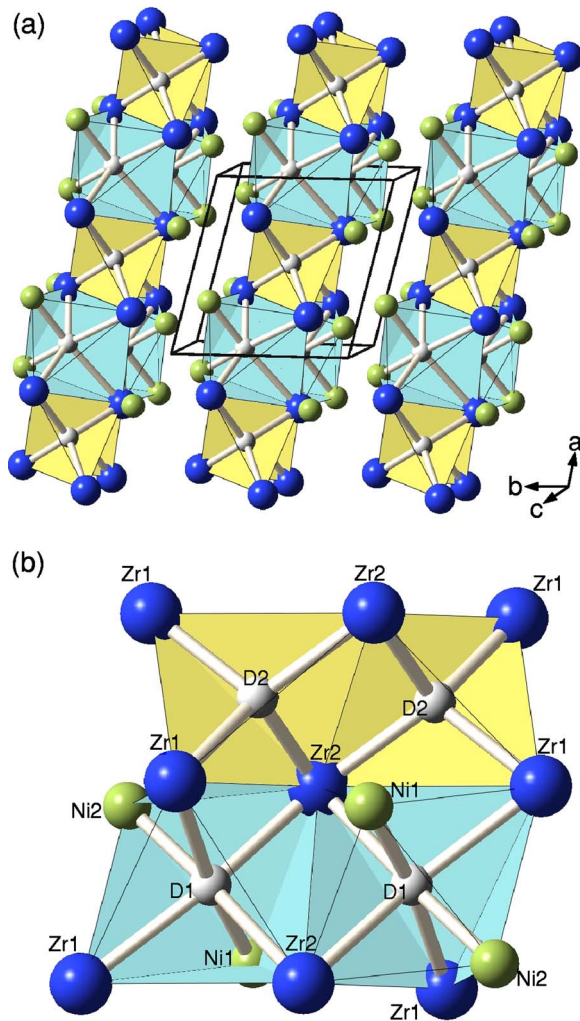


FIG. 2. (Color online) (a) Crystal structure of β -ZrNiD_{1-x} viewed in a near-projection along the **c** axis. Large dark (blue) and small light (green) spheres denote Zr and Ni atoms, respectively. Small white spheres denote D atoms in the shaded polyhedra. (b) Local configuration of Zr₄-tetrahedral and Zr₄Ni₂-octahedral interstitial D sites viewed in a near-projection along the **b** axis. The metal-deuterium bond distances are listed in Table III.

are shortened. The Ni-D2 bond lengths are also much longer than the four Zr-D2 bond lengths, which are within the range of 2.064(5)–2.135(4) Å. Therefore, the D2 site is more reasonably described as a “Zr₄ site,” which is indeed crystallographically distinct from the D1 site. The Zr₄ D2 tetrahedra (2 per unit cell) are fairly symmetric with Zr-D2-Zr bond angles in the range of 100.37(18)–119.81(15)°, close to the 109.47° dihedral angles of a regular tetrahedron. From the refined crystal structure (Fig. 2), the different deuterium sites apparently yield an ordered arrangement of alternating Zr₄Ni₂ D1 octahedra and Zr₄ D2 tetrahedra along the **a** axis. Such alternately ordered columns of octahedra and tetrahedra propagate along the **c** axis so as to form sheets of edge-shared polyhedra normal to the **b** axis. Each polyhedron shares its Zr-Zr edge with only four other polyhedra due to the dimensional behavior in this structure. The shortest D-D distance in this configuration is 2.559(7) Å, which satisfies the Switendick criterion.³⁰

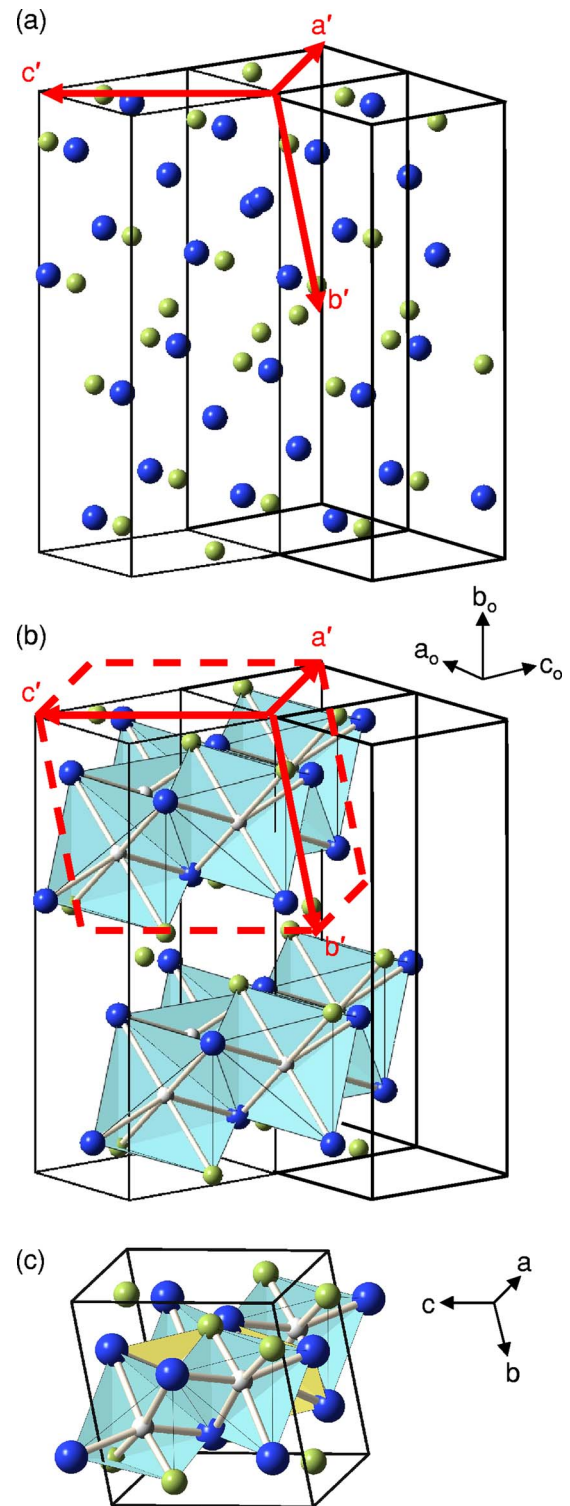


FIG. 3. (Color online) Structure comparison between (a) $Cmcm$ ZrNi, (b) $Cmcm$ ZrNiD and (c) $P\bar{1}$ ZrNiD. Large dark (blue) and small light (green) spheres denote Zr and Ni atoms, respectively. Small white spheres denote D atoms in the shaded polyhedra. The axes of the orthorhombic structure are indicated with subscript “o.”

Figure 3 illustrates a possible $Cmcm \leftrightarrow P\bar{1}$ phase transition path between the α -ZrNi alloy and the β -ZrNi deuteride phase during the absorption process [see Fig. 3(a)]:

$\mathbf{a} \approx \mathbf{a}_0 + \mathbf{c}_0$, $\mathbf{b} \approx (\mathbf{a}_0 + \mathbf{b}_0)/2$, $\mathbf{c} = \mathbf{a}_0 + (-\mathbf{c}_0)$, $\alpha = \mathbf{b} \wedge \mathbf{c}$, $\beta = \mathbf{c} \wedge \mathbf{a}$, $\gamma = \mathbf{a} \wedge \mathbf{b}$. According to Westlake *et al.*,³ β -ZrNiD has a *Cmcm* structure similar to α -ZrNi, with interstitial D atoms occupying the Zr_4 site or as the later suggested, the more plausible “ Zr_4Ni_2 site.”²¹ Therefore, it is likely that the proposed $Cmcm \Leftrightarrow P\bar{1}$ phase transform path may also be applied to relations between the previously reported *Cmcm* ZrNiD and the present $P\bar{1}$ ZrNiD structure [see Fig. 2(b)]. It is known that the formation of a particular crystal structure is sometimes intimately dependent on the preparation conditions, although this structure may not necessarily have the lowest energy among all possible polymorphs of this compound. Nonetheless, the present NPD investigation of ZrNiD_{0.88} from 10 K–300 K did not reveal any evidence of possible phase transitions. Thus, it is probable that the $P\bar{1}$ structure is the only stable form for β -ZrNiD_{1-x}.

The relative stabilities of the present $P\bar{1}$ structure and the previously reported *Cmcm* structure were investigated by first-principles DFT calculations. Both structures were fully relaxed during the calculations with respect to lattice parameters and atomic positions. The total energy calculated for the optimized $P\bar{1}$ ZrNiD structure was found to be ≈ 0.24 eV per unit cell lower than that for the optimized *Cmcm* ZrNiD structure. Adding the zero-point contributions to the total energies resulted in a free-energy difference of ≈ 0.21 eV per unit cell; i.e., the $P\bar{1}$ phase is still more stable than the *Cmcm* structure, in agreement with the current NPD results.

In seeking an explanation for the current triclinic structure being the lowest-energy configuration, it is useful to consider the local bonding configurations in both forms of ZrNi monodeuteride. Although the derived structure from the *Cmcm* lattice shows some similarities with the triclinic $P\bar{1}$ structure, there are significant differences in the local bonding coordination of each D interstitial site. Figure 4 shows the total electron densities of states (DOS) and their projections around the different atomic sites for the $P\bar{1}$ ZrNiD structure. The prominent (≈ 3.3 eV width) low-energy feature observed in the total DOS (centered about 7 eV below the Fermi energy, E_F) corresponds to metal-D1 and metal-D2 bands. In contrast to the low-energy, single-band (≈ 2.6 eV width) structure calculated for *Cmcm* ZrNiH,⁶ where all four Zr_4Ni_2 sites are identical, the low-energy feature for the $P\bar{1}$ structure actually contains two distinct bands associated with the two different D sites. From the DOS projections around the different atom sites, the DOS for the Zr_4 -site deuterium is almost the same as that for *Cmcm* ZrNiH,⁶ and the M-D interactions are dominated mainly by the Zr-D bonding for this site, with the Ni-D interaction being much weaker. The lower-energy DOS for the Zr_4Ni_2 -site deuterium corresponds not only to the strong Zr-D interaction but also to the increased Ni-D bonding associated with the significantly reduced Ni-D bond length. The Ni-H(D) bonds in the Zr_4Ni_2 site are shortened from 2.246 Å (*Cmcm*, Ref. 3) to 1.810(4) and 1.876(4) Å ($P\bar{1}$). The total DOS band structure at higher energy is similar to that in *Cmcm* ZrNiH,⁶ where a strong band of ≈ 4.0 eV width is mostly due to the DOS of the Ni-3d localized states, and the Zr-4d states are more delo-

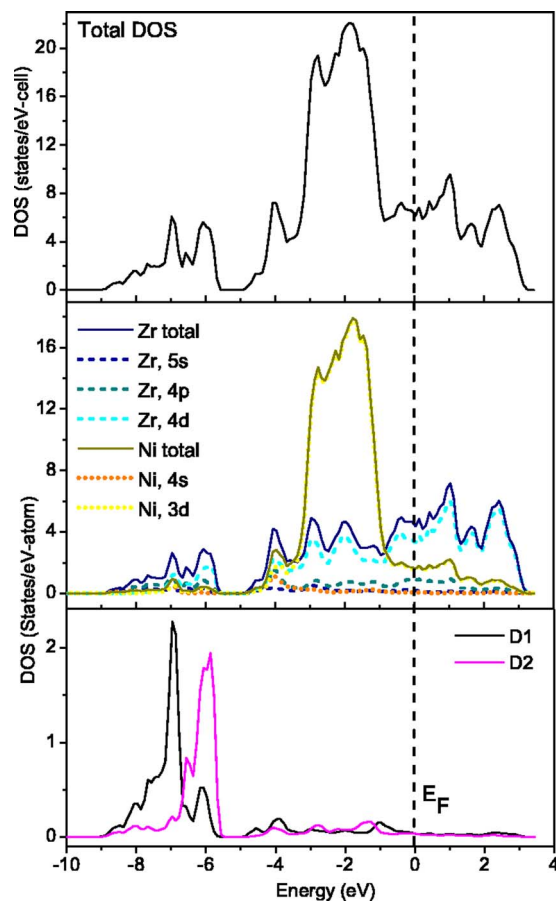


FIG. 4. (Color online) Total electronic DOS of $P\bar{1}$ ZrNiD and projection around the different atomic sites. The *l*-projected DOS of Zr and Ni are also shown. D1 atoms occupy Zr_4Ni_2 sites and D2 occupy Zr_4 sites. E_F is taken as the zero of energy and shown as the dashed line.

calized, which results in much broader bands of lower DOS. The top of the Ni-*d* bands is ≈ 0.8 eV lower than E_F , and the Zr-*d* contributions at and above E_F are much larger than those of the Ni-*d* state. As previously proposed,^{5,6} since the Ni-*s*, *p*, and *d* states that participate in the metal-D bonding were already occupied in pure ZrNi, the Zr-D interaction plays a crucial role in stabilizing the β -deuteride phase by lowering the energy of the empty Zr-*d* states in pure ZrNi below the Fermi level of the deuteride, and also because of the larger energy gain resulting from the lowering of the higher-energy Zr-4d states compared to the Ni-3d states. In that sense, the total energy of the $P\bar{1}$ structure would be further lowered because the Zr-D binding in the Zr_4 sites becomes even stronger due to the dramatically decreased Zr-H(D) bond lengths, from 2.175–2.25 Å (*Cmcm* structure)³ to 2.064(5)–2.135(4) Å (Table III). We believe that these differences in the local-bonding arrangements are largely responsible for the free-energy difference between the $P\bar{1}$ and *Cmcm* structures. In addition, the Zr-D bond lengths for the Zr_4 site are much shorter than those for the Zr_4Ni_2 site (Table III). Therefore the stronger binding with deuterium makes the D2 (Zr_4 site) more stable, leading to higher D2 occupancies in the $P\bar{1}$ cell. With increasing D content toward ZrNiD,

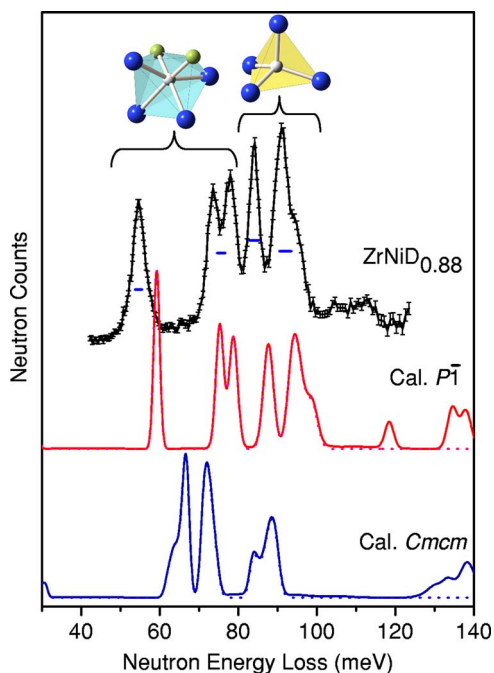


FIG. 5. (Color online) NV spectrum of $\text{ZrNiD}_{0.88}$ at 10 K. FWHM instrumental resolutions are depicted by the horizontal bars beneath the spectra. Calculated spectra for $P\bar{1}$ and $Cmcm$ β - ZrNiD delineating both 1 phonon (dotted line) and 1+2 phonon (solid line) contributions are shown with the experimental data.

a two-phase region is reached with the appearance of γ - ZrNiD_3 .^{11,12} This is further evidence that the Zr_4Ni_2 site is less stable, since such a site will have a greater probability of being occupied in β - ZrNiD_{1-x} as $x \rightarrow 0$ (i.e., as the D content increases). For D contents approaching and above the monodeuteride stoichiometry, the repulsive D-D interaction at short distance would be chiefly responsible for the onset and formation of the trideuteride γ phase.

The observed phonon density of states for $\text{ZrNiD}_{0.88}$ was also found to corroborate the refined $P\bar{1}$ structure. Figure 5 shows the NV spectrum for $\text{ZrNiD}_{0.88}$ at 10 K, which displays six peaks. To understand the spectra, we performed first-principle phonon calculations. We started with the optimized ZrNiD $P\bar{1}$ structure mentioned earlier. The relaxed atomic positions agreed closely with our experimental values for β - $\text{ZrNiD}_{0.918}$. The phonon calculations were then performed with this optimized structure. A cell of $1a \times 1b \times 1c$ was used and the full dynamical matrix was obtained from a total of 36 symmetry-independent atomic displacements (0.01 Å). The computed phonon dispersion and phonon density of states are shown in Fig. 6. The ZrNiD NV spectrum was computed for a $10 \times 10 \times 10$ q -point grid within the incoherent approximation with instrumental resolution taken into account.³¹ The primitive cell of ZrNiD contains 4 formula units (i.e., 12 atoms) giving rise to a total of 36 phonon branches (18 A_g and 18 A_u). Inspection of the eigenvectors allows the characterization of the modes. The NV spectrum is dominated by D-atom displacements. NV intensities largely associated with the metal-atom displacements (peaks between 0 and 30 meV) were not measured. In Fig. 5, the

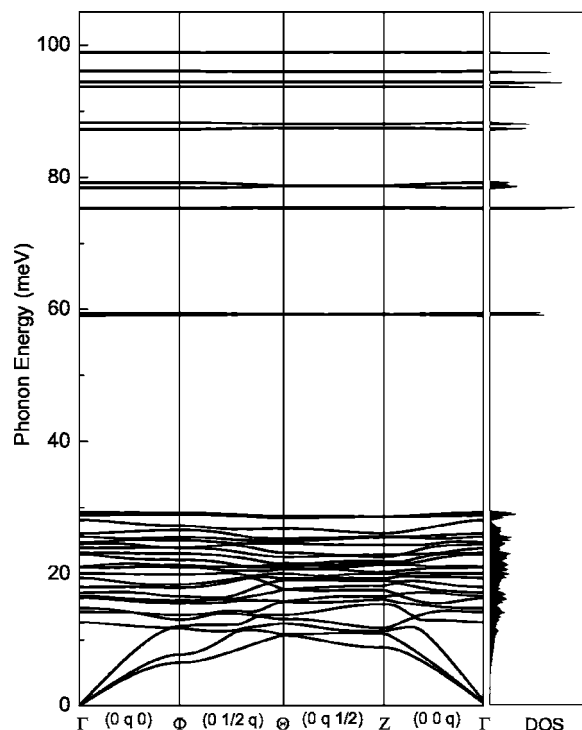


FIG. 6. Calculated phonon dispersion curves along high-symmetry directions in the Brillouin zone for $P\bar{1}$ β - ZrNiD . The phonon density of states is also shown.

first three modes at ≈ 54.6 , 73.5, and 78.1 meV originated from D atoms in the Zr_4Ni_2 D1 octahedral sites with the lowest peaks assigned to D vibrations along the Zr2-D1-Ni2 direction (*N.B.*: Zr2-D1 has the longest bond lengths in the octahedron). The other higher modes at ≈ 84.0 , 90.8, and 95.3 meV were from D atoms in the Zr_4 D2 tetrahedral sites, which contain much shorter Zr-D bonds. An NV spectrum based on the previously reported $Cmcm$ structure³ was also simulated (see Fig. 5), and it is clearly unlike the measured $\text{ZrNiD}_{0.88}$ spectrum.

From Fig. 5, the calculated phonon modes for $P\bar{1}$ β - ZrNiD agree reasonably well overall with the observed NV spectrum of $\text{ZrNiD}_{0.88}$, although the calculations are found to overestimate the position of the lowest-energy feature. In particular, the phonon energy of the observed NV peak is centered at ≈ 54.6 meV while the calculated energy is ≈ 7 meV higher. According to our calculations, this peak consists of two phonon modes corresponding to the octahedral D atom vibrating along the longest Zr-D and Ni-D bonds, in-phase and out-of-phase, respectively. Our frozen-phonon calculation for these two specific modes show that the in-phase mode is harmonic, but the out-of-phase mode is strongly anharmonic with an asymmetric energy vs D displacement potential curve. We believe that this anharmonicity is responsible for the energy discrepancy between calculation and experiment. Further investigation is necessary to understand this interesting behavior. Moreover, in the measured sample, the octahedral sites are not completely occupied. Our first-principles phonon calculations are based on a structure with complete occupancies for all atoms, which would probably result in stronger M-D interactions. There-

fore, calculated phonon energies might be expected to be somewhat higher than the observed modes. Nonetheless, the observed and calculated NV spectra are generally consistent with the refined structure determined from the NPD data and further confirm that there are two crystallographically distinct deuterium sites in the β -ZrNiD_{1-x} structure, not just one site as proposed previously. It should be noted that, although this study was performed with deuterium, all structural and spectroscopic results are directly applicable to β -ZrNiH_{1-x}, as further evidenced by the similar NV spectrum reported for ZrNiH_{0.88}.¹²

IV. CONCLUSIONS

We have directly solved the structure of β -phase ZrNi deuteride via Rietveld model refinements of the NPD patterns for ZrNiD_{0.88} and ZrNi(H_{0.64}D_{0.36})_{0.88}. The 300 K refinement indicates a β -ZrNiD_{0.918} stoichiometry with a triclinic $P\bar{1}$ structure and lattice parameters: $a=5.2637(1)$ Å, $b=5.3752(2)$ Å, $c=5.2264(1)$ Å, $\alpha=101.521(3)^\circ$, β

$=100.663(2)^\circ$, and $\gamma=100.590(3)^\circ$. In contrast to the previously proposed orthorhombic ($Cmcm$) or slightly distorted quasi- $Cmcm$ ZrNiD with a single D site, the true β -phase structure contains two crystallographically distinct D sites: Zr₄Ni₂ octahedral sites and Zr₄ tetrahedral sites, alternately ordered along the **a** direction. As shown by first-principles calculations, this energetically favored triclinic structure is also in general agreement with the ZrNiD_{0.88} neutron vibrational spectrum and consistent with the electronic structure predictions.

ACKNOWLEDGMENTS

The authors appreciate the assistance of M. Prina with preparation of the ZrNiD_{0.88} sample at JPL. This work was partially supported by DOE through EERE Grant No. DE-AI-01-05EE11104 and BES Grant No. DE-FG02-98ER45701, and was partially performed at the Jet Propulsion Laboratory, California Institute of Technology, under a contract with the National Aeronautical and Space Administration.

*Author to whom all correspondence should be addressed. Electronic address: huiwu@nist.gov

¹W. L. Korst, J. Phys. Chem. **66**, 370 (1962).

²S. W. Peterson, V. N. Sadana, and W. L. Korst, J. Phys. (Paris) **25**, 451 (1964).

³D. G. Westlake, H. Shaked, P. R. Mason, B. R. McCart, and M. H. Mueller, J. Less-Common Met. **88**, 17 (1982).

⁴R. Kronski and T. Schober, J. Alloys Compd. **205**, 175 (1994).

⁵M. Gupta, J. Alloys Compd. **293**, 190 (1999).

⁶N. Michel, S. Poulat, P. Millet, P. Dantzer, L. Priester, and M. Gupta, J. Alloys Compd. **330**, 280 (2002).

⁷D. G. Westlake, J. Less-Common Met. **75**, 177 (1980).

⁸I. Jacob and J. M. Bloch, Solid State Commun. **42**, 541 (1982).

⁹M. J. Benham, J. D. Browne, and D. K. Ross, J. Less-Common Met. **103**, 71 (1984).

¹⁰S. Yang, F. Aubertin, P. Rehnbein, and U. Gonser, Z. Kristallogr. **195**, 281 (1991).

¹¹N. L. Adolphi, S. Badola, L. A. Browder, and R. C. Bowman, Jr., Phys. Rev. B **65**, 024301 (2001); N. L. Adolphi, S. Badola, L. A. Browder, and R. C. Bowman, *ibid.* **69**, 149901(E) (2004).

¹²R. C. Bowman, Jr., N. L. Adolphi, S.-J. Hwang, J. G. Kulleck, T. J. Udovic, Q. Huang, and H. Wu, Phys. Rev. B **74**, 184109 (2006).

¹³G. G. Libowitz, H. F. Hayes, and T. R. P. Gibb, Jr., J. Phys. Chem. **62**, 76 (1958).

¹⁴W. Luo, A. Craft, T. Kuji, H. S. Chung, and T. B. Flanagan, J. Less-Common Met. **162**, 251 (1990).

¹⁵J. S. Cantrell, R. C. Bowman, Jr., L. A. Wade, S. Luo, J. S. Clewley, and T. B. Flanagan, J. Alloys Compd. **231**, 518 (1995).

¹⁶P. Dantzer and P. Millet, Rev. Sci. Instrum. **71**, 142 (2000).

¹⁷T. Kabutomori, Y. Wakisaka, K. Tsuchiya, and H. Kawamura, J.

Nucl. Mater. **258**, 481 (1998).

¹⁸B. D. Freeman, E. L. Ryba, R. C. Bowman, Jr., and J. R. Phillips, Int. J. Hydrogen Energy **22**, 1125 (1997).

¹⁹R. C. Bowman, Jr., J. Alloys Compd. **356**, 789 (2003).

²⁰M. Prina, R. C. Bowman, Jr., and J. G. Kulleck, J. Alloys Compd. **373**, 104 (2004).

²¹S. J. C. Irvine, D. K. Ross, I. R. Harris, and J. D. Browne, J. Phys. F: Met. Phys. **14**, 2881 (1984).

²²J. K. Stalick, E. Prince, A. Santoro, I. G. Schroder, and J. J. Rush, in "Neutron Scattering in Materials Science II," Mat. Res. Soc. Symp. Proc. edited by D. A. Neumann, T. P. Russell, and B. J. Wuensch, Vol. 376 (Materials Research Society, Pittsburgh, PA, 1995), p. 101.

²³A. C. Larson and R. B. Von Dreele, "General Structure Analysis System," Report LAUR 86-748. Los Alamos National Laboratory, NM, 1994.

²⁴T. J. Udovic, D. A. Neumann, J. Leão, and C. M. Brown, Nucl. Instrum. Methods Phys. Res. A **517**, 189 (2004).

²⁵S. Baroni, A. Dal Corso, S. de Gironcoli, and P. Giannozzi, <http://www.pwscf.org>.

²⁶G. Kresse, J. Furthmuller, and J. Hafner, Europhys. Lett. **32**, 729 (1995).

²⁷T. Yildirim, Chem. Phys. **261**, 205 (2000).

²⁸J. K. Stalick (private communication).

²⁹M. E. Kirkpatrick, D. M. Bailey, and J. F. Smith, Acta Crystallogr. **15**, 252-255 (1962).

³⁰A. C. Switendick, Theoretical study of hydrogen in metals: Current status and further prospects, SAND 78-0250, 1978.

³¹G. L. Squires, *Introduction to the Theory of Thermal Neutron Scattering* (Dover, New York, 1996).